ACS Catalysis

Research Article

pubs.acs.org/acscatalysis

Highly Dispersed Copper Oxide Clusters as Active Species in Copper-Ceria Catalyst for Preferential Oxidation of Carbon Monoxide

Wei-Wei Wang,[†] Pei-Pei Du,[‡] Shi-Hui Zou,[†] Huan-Yu He,[†] Rui-Xing Wang,[†] Zhao Jin,[†] Shuo Shi,[§] Yu-Ying Huang,[‡] Rui Si,*[,‡] Qi-Sheng Song,[†] Chun-Jiang Jia,*[,†] and Chun-Hua Yan[§]

[†]Key Laboratory for Colloid and Interface Chemistry, Key Laboratory of Special Aggregated Materials, School of Chemistry and Chemical Engineering, Shandong University, Jinan 250100, China

[‡]Shanghai Synchrotron Radiation Facility, Shanghai Institute of Applied Physics, Chinese Academy of Sciences, Shanghai 201204, China

[§]Beijing National Laboratory for Molecular Sciences, State Key Lab of Rare Earth Materials Chemistry and Applications, PKU-HKU Joint Lab in Rare Earth Materials and Bioinorganic Chemistry, Peking University, Beijing 100871, China

Supporting Information

ABSTRACT: Copper-ceria is one of the very active catalysts for the preferential oxidation of carbon monoxide (CO-PROX) reaction, which is also a typical system in which the complexity of copper chemistry is clearly exhibited. In the present manuscript, copper−ceria catalysts with different Cu contents up to 20 wt % supported on CeO_2 nanorods were synthesized by a deposition−precipitation (DP) method. The as-prepared samples were characterized by various structural and textural detections including X-ray diffraction (XRD), Vis-Raman, transmission electron microscopy (TEM), *ex situ*/*in situ* X-ray absorption fine structure (XAFS), and temperature-programmed reduction by hydrogen (H_2-TPR). It has been confirmed that the highly dispersed copper oxide (CuO_x) clusters, as well as the strong interaction of Cu-[O_x]-Ce structure, were the main copper species deposited onto the ceria surface. No separated copper phase was detected for both preoxidized and prereduced samples with the Cu contents up to 10 wt %. The fresh copper−ceria catalysts were pretreated in either O_2- or H_2-atmosphere and then tested for the CO-PROX reaction at a space velocity (SV) of 60 000 mL·h^{-1}·$g_{cat}$$^{-1}$. The prereduced 5 and 10 wt % Cu samples exhibited excellent catalytic performance with high CO conversions (>50%, up to 100%) and O_2 selectivities (>60%, up to 100%) within a wide temperature window of 80−140 °C. The *in situ* XAFS technique was carried out to monitor the structural evolution on the copper−ceria catalysts during the PROX experiments. The X-ray absorption near edge spectra (XANES) profiles, by the aid of linear combination analysis, identified the oxidized Cu(II) were the dominant copper species in both O_2- and H_2-pretreated samples after CO-PROX at 80 °C. Furthermore, the extended X-ray absorption fine structure (EXAFS) fitting results, together with the corresponding H_2-TPR data distinctly determined that the highly dispersed CuO_x (x = 0.2−0.5) cluster, other than the Cu−[O_x]−Ce (x = 0.7−3.2) structure, were the crucial active species for the studied CO-PROX reaction.

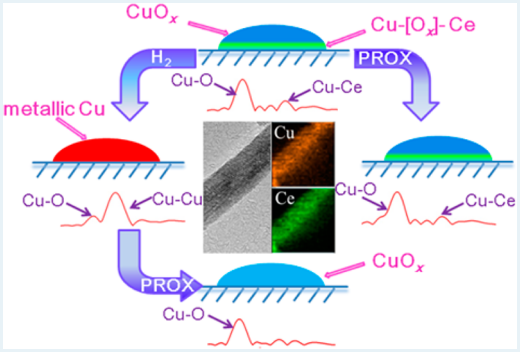

KEYWORDS: *copper oxide catalyst, preferential oxidation of CO, X-ray absorption fine structure, ceria support, in situ characterization, structure−activity relationship*

1. INTRODUCTION

The polymer−electrolyte−membrane fuel cell, which is accompanied by multistep reactions including the hydrocarbon reforming and the water−gas shift reactions, is an efficient approach toward the application of hydrogen energy, substituting the current fossil fuels. However, a small amount (0.3−1%) of carbon monoxide (CO) remaining in the hydrogen inlets will be severely poisonous to the platinum catalyst, which is popularly used for the hydrogen oxidation reaction at the anode of proton exchange membrane fuel cells.[1,2] Therefore, the preferential oxidation of CO (CO-PROX) in the excess of H_2 is a key to effectively eliminate the toxic CO molecules.[3] In recent studies, diverse noble metals (NMs) such as Pt,[4−10] Au,[7,11,12] Ru,[9,10,13] Ir,[8] Pd,[8,9] and Rh[10] have displayed their potential ability to the CO-PROX process. However, the low O_2 selectivity (<60%)[6−8] and economic issues prevent the wide application of NM catalysts. Recently, the fundamental research on cerium oxide (CeO_2)-supported copper oxide (CuO) catalyst has demonstrated that the copper−ceria (Cu−Ce−O) system is a very promising candidate for the CO-PROX reaction at the temperature range of 100−140 °C not only because of superiority in both

Received: September 30, 2014
Revised: February 5, 2015
Published: February 13, 2015

DOI: 10.1021/cs5014909
ACS Catal. 2015, 5, 2088−2099

CO conversion (60−100%) and O_2 selectivity (60−100%) but also due to the much lower cost than the NMs.[7,14−17]

During the last several decades, copper−ceria catalysts have been synthesized through different chemical approaches including deposition−precipitation,[12] incipient wetness impregnation,[14,18,19] coprecipitation,[12,16,18,20] and the sol−gel method.[20] By the aids of these controlled preparation strategies, various structural and textural characteristics have been realized on the reported copper−ceria samples previously. However, until now, the structure−activity relationship on Cu−Ce−O system has not been clearly addressed in catalysis, possibly due to the structural complexities of the copper/ceria phase (Cu/Cu_2O/CuO, Ce^{3+}/Ce^{4+}, etc.), as well as the presence of copper oxide clusters (CuO_x) weakly or strongly interacting with the CeO_2 support under the nanosize scale. On the other hand, multiple characterization techniques such as Raman,[19,21] X-ray photoelectron spectroscopy (XPS),[12,17] temperature-programmed reduction (TPR),[12,16,19] and diffuse reflectance infrared Fourier transform spectroscopy (DRIFTS)[18,19,22] have been extensively applied to the copper−ceria catalysts, as powerful detection means to identify active sites and explore reaction mechanisms for the CO-PROX reaction. For instance, by using in situ DRIFTS measurements, Polster et al. found that the CO oxidation activity is linked to Cu^+ carbonyl species (~2110 cm^{-1}), whereas the deactivation process is associated with the catalyst hydration.[22]

The *in situ* X-ray absorption fine structure (XAFS) technique has been broadly used in structural evolution on nanostructured catalysts,[18,23] particularly for the determination of active metal/metal oxide species. XAFS, which includes X-ray near edge structure (XANES) and extended X-ray absorption fine structure (EXAFS), is very effective for the determination of both electronic properties (oxidation state, charge transfer, etc.) and short-range local structure (coordination number, bond distance, Debye−Waller factor, etc.), respectively, of solids in heterogeneous catalysis. For the copper−ceria catalyst on the CO-PROX reaction, by extensively using *in situ* DRIFTS and XANES tests[18,24−26] as strong experimental evidence, several groups have reported the corresponding "structure−activity" relationship (i.e., the active site,[18,26] the deactivation mechanism,[25] and the interaction of CeO_x/CuO in inverse catalyst,[24] etc.). All these studies demonstrated that active sites in copper−ceria oxide system for the CO oxidation are related to interfacial Cu(I) species generated through a reductive process upon interaction with the CO. Very recently, Yao et al. reported the operando combined XANES/DRIFTS technique to reveal the mechanism of the CO + O_2 process (3.3%CO/1.7%O_2/He, no presence of H_2), without H_2, on the CuO/CeO_2 catalyst, and demonstrated that the surface dispersed Cu(I) species rather than Cu(0) were active species for the CO oxidation reaction,[27] which is consistent with the active site identifications in CO-PROX reaction.[18,24−26] However, details on the local structure of active Cu-O sites in working CO-PROX catalyst have been rarely explored. Recently, using *in situ* EXAFS, Zhang et al. identified the local coordination of the active redox oxygen ions in CO-PROX reaction and the related active Cu species in a mixed copper cerium oxide catalyst.[28] They confirmed that the active/labile oxygen is the first oxygen neighbor of Cu(II) species those isolate with CeO_2 in a mixed oxide solution ($CuCeO_x$).

Furthermore, the reducibility and surface properties of copper−ceria catalyst have been confirmed to be complicated and usually contributed by multiple oxidized copper species, such as CuO_x clusters, Cu−[O_x]−Ce structure and Cu^{2+} ion in the CeO_2 lattice by the confirmation of H_2-TPR.[12,19,21,29] This also has resulted in the presence of debates about different hypotheses on the active species for the CO-PROX reaction. Therefore, in this paper, we have tried to obtain active copper−ceria catalysts by depositing the highly dispersed CuO_x clusters onto the CeO_2 nanorods. The as-prepared copper−ceria catalysts via controlled synthesis and pretreatment have shown excellent catalytic performance (i.e., CO conversion >50% and O_2 selectivity >60%, within the wide temperature range of 80−140 °C). By using the *in situ* XANES/EXAFS techniques, with the aids of XRD, Vis-Raman, TEM and H_2-TPR characterizations, the highly dispersed CuO_x cluster, rather than the strong interaction of Cu−[O_x]−Ce structure, has been identified as the more crucial active species in Cu−Ce−O system for CO-PROX.

2. EXPERIMENTAL SECTION

2.1. Synthesis of Catalysts. All the reactants are of analytical grade and were used without further purification or modification. Cerium nitrate ($Ce(NO_3)_3·6H_2O$, 99.5%) and copper nitrate ($Cu(NO_3)_2·3H_2O$, 98.0−102.0%) were purchased from Tianjin Kermal Chemical Reagent Factory. Sodium hydroxide (NaOH, ≥96.0%) was purchased from Sinopharm Chemical Reagent Factory. Sodium carbonate (Na_2CO_3, 99.8%) was obtained from Tianjin BoDi Chemical Reagent Factory. The copper−ceria catalysts were prepared by a DP method according to the previous report.[29] First, rod-like ceria support was obtained via a controlled hydrolysis procedure, followed by a hydrothermal treatment.[30] In a typical synthesis, 1.30 g of $Ce(NO_3)_3·6H_2O$ and 14.40 g of NaOH were dissolved in 20 and 40 mL of deionized water, respectively. Then, the two solutions were mixed in a 100 mL Teflon bottle, and stirred for 30 min. Next, the Teflon bottle was held in a stainless steel vessel autoclave and sealed tightly, and then the autoclave was subjected to hydrothermal treatment at 100 °C for 24 h. The obtained precipitates were separated by centrifugation, washed with deionized water and ethanol several times, and then dried at 60 °C overnight. For the sequential DP synthesis, the ceria powders (0.50 g) were suspended in 25 mL Millipore water (18.25 MΩ) under stirring. Various amounts of copper precursor, $Cu(NO_3)_2·3H_2O$, were dissolved in 12.5 mL of Millipore water and then added into the above CeO_2/H_2O suspension dropwisely. During the whole process, the pH value of the stock solution was controlled to ca. 9 by adding Na_2CO_3 aqueous solution (0.50 $mol·L^{-1}$). The green precipitates were further aged at room temperature for 1 h before filtration and then washed by Millipore water (1 L) at room temperature. The product was dried in air at 75 °C overnight and then calcined in still air at 400 °C for 4 h (heating rate: 2 °C·min^{-1}). In this work, the copper−ceria samples were donated as ***a*CuCe** (a = 2, 5, 10 and 20), where a is the copper content in weight percent (a = [Cu/CeO_2]$_{wt}$ × 100%).

2.2. Characterization of Catalysts. The copper loadings were determined by inductively coupled plasma atomic emission spectroscopy (ICP-AES) on an IRIS Intrepid II XSP instrument (Thermo Electron Corporation). The nitrogen adsorption−desorption measurements were performed on a NOVA 4200e instrument at 77 K. All the copper−ceria samples were degassed at 150 °C under vacuum for over 6 h. The BET specific surface area was calculated from the adsorption data in the relative pressure range between 0.05 and 0.20. X-ray

DOI: 10.1021/cs5014909
ACS Catal. 2015, 5, 2088−2099

Table 1. Copper Contents (Cu), BET Specific Surface Areas (S_{BET}), H_2-TPR Reduction Temperatures (T_R) and H_2-Consumption (H_2), Ratio of Oxygen to Copper (O/Cu), CO-PROX Reaction Conversions (CO conv.) and Selectivities (O_2 select.) of Copper−Ceria Samples

	Cu	S_{BET}	T_R	H_2	O/Cu[d]	CO conv. (%)		O_2 select. (%)	
sample	(wt %)[a]	(m^2g^{-1})	(°C)[b]	(μmol·g^{-1})[c]		O_2[e]	H_2[f]	O_2[e]	H_2[f]
2CuCe	1.5	92	[α]189, [β]228	[α]108, [β]751 [γ](236)	[α]0.46, [β]3.18	15	30	84	90
5CuCe	4.9	97	161, 190	274, 1035 (721)	0.36, 1.34	48	70	99	98
10CuCe	10.1	90	139, 167	442, 1465 (1405))	0.28, 0.92	65	72	100	100
20CuCe	17.6	80	157, 181	671, 1880 (2256)	0.24, 0.68	41	41	98	100

[a]Determined by ICP-AES. [b]Left: low-temperature reduction peak (α); Right: high-temperature reduction peak (β). [c]Low-temperature (α) and high-temperature (β) of actual value of H_2-consumptions; (γ): theoretic values of H_2 consumption calculated according to $Cu^{2+} \rightarrow Cu^0$; (δ): number of total surface oxygen per Cu based on the copper content and calculated H_2-consumption. [d]Number of total oxygen per Cu based on calculated H_2-consumption in TPR, (α): from low-temperature reduction peak (highly dispersed CuO_x cluster), (β): from high-temperature reduction peak (Cu-[O_x]-Ce structure). [e]Activity measured at 80 °C in 1%CO/1%O_2/50%H_2/N_2 after the O_2-pretreatment. [f]Activity measured at 80 °C in 1%CO/1%O_2/50%H_2/N_2 after the H_2-pretreatment.

Diffraction (XRD) was operated on a Bruker D8 Advance diffractometer (40 kV, 40 mA), using Cu Kα radiation (λ = 0.15406 nm). The powder catalyst after grinding was placed inside a quartz-glass sample holder before test. Raman spectra were acquired by excitation of the sample at 532 nm using a Raman microscope system (HORIBA JOBIN YVON) in the spectral window from 100 to 800 cm^{-1} with a spectral resolution of 2 cm^{-1}. Transmission electron microscopy (TEM) and high-resolution TEM (HRTEM) were conducted on a Philips Tecnai F20 instrument at 200 kV. All the investigated samples were sonicated in ethanol before being dropped on an ultrathin carbon film-coated Mo grid. For the corresponding elemental mapping acquisition, the energy dispersive spectroscopy (EDS) was applied to the measured catalysts under the scanning transmission electron microscopy (STEM) mode on the same TEM machine.

Temperature-programmed reduction by hydrogen (H_2-TPR) was carried out in a Builder PCSA-1000 instrument equipped with a thermal conductivity detector (TCD) to detect H_2 consumption. The sieved catalysts (20−40 mesh, 30 mg) were heated (5 °C/min) from room temperature to 400 °C in a 5% H_2/Ar (30 mL·min^{-1}) gas mixture. Before each measurement, the fresh samples were pretreated in pure O_2 at 300 °C for 30 min, and the reduction samples were pretreated in 5%H_2/Ar at 300 °C for 2 h.

The *ex situ* Cu K absorption edge (E_0 = 8979 eV) XAFS spectra were collected in transmission mode at BL14W1 beamline of the Shanghai Synchrotron Radiation Facility (SSRF) operated at 3.5 GeV under "top-up" mode with a constant current of 220 mA. The *in situ* experiments were conducted at the X18B beamline of the National Synchrotron Light Source (NSLS) at Brookhaven National Laboratory (BNL), operated at 2.8 GeV under "decay" mode with currents of 160−300 mA. The powder sample (~16 mg) was loaded into a Kapton tube (o.d. = 1/8 in.), which was attached to an *in situ* flow cell. Two small resistance heating wires were installed above and below the tube, and the temperature was monitored with a 0.5 mm chromel−alumel thermocouple that was placed inside the tube near the sample. The *in situ* PROX reaction (1% CO/1%O_2/50%H_2/He, 20 mL·min^{-1}) was carried out under a "steady-state" mode at 80 °C for 1 h. Each XAFS spectrum was taken under fluorescence mode with a Pips detector and accumulated by multiple (>12) scans (ca. 20 min each). No distinct changes were observed between the first and the last scans. The reported XAFS data were the averages of these scans collected after cooling the tested sample down to room temperature in the same pretreatment/reaction atmosphere.[31] The XANES and EXAFS data have been analyzed via Athena and Artemis programs.

2.3. Catalytic Tests. The CO-PROX reactivity was tested in a plug-flow reactor by using 50 mg of sieved catalyst (20−40 mesh) in a gas mixture of 1%CO/1%O_2/50%H_2/N_2 with a space velocity of 60 000 mL·h^{-1}·g_{cat}^{-1}. Prior to the measurement, the tested sample was pretreated in oxidative (21%O_2/N_2) or reductive (50%H_2/N_2) atmospheres at 300 °C for 30 min before the beginning of activity test experiments as described below. For a typical catalytic run, the copper−ceria sample was heated from 40 to 200 °C and was stabilized at each temperature plateau under the same reaction conditions for 40 min to reach the equilibrium. The compositions of the effluent gases were measured with an online gas chromatograph (GC 9160 series) equipped with a thermal conductivity detector. Two column channels in the GC were used to separate the tested gases. One channel was coupled to a column of Molsieve 5 Å to separate CO, O_2, and N_2, and the other channel was attached a column of PoraPLOT N to isolate CO_2. Considering that the total volumes of the reaction gas before and after PROX changed very slightly (<1 vol %), the CO conversions and O_2 selectivities were calculated according to the following equations:

$$\text{CO conversion (\%)} = (n_{CO,in} - n_{CO,out})/n_{CO,in} \times 100$$

$$O_2 \text{ selectivity (\%)} = 0.5 \times (n_{CO,in} - n_{CO,out})/(n_{O2,in} - n_{O2,out}) \times 100$$

where $n_{CO,in}$ and $n_{O2,in}$ are the corresponding GC response peak area values of the inlet gas of CO and O_2, respectively, before the reactor, whereas $n_{CO,out}$ and $n_{O2,out}$ are the corresponding GC response peak area values of CO and O_2, respectively, after the reactor.

3. RESULTS AND DISCUSSION

3.1. Structure and Texture of Copper−Ceria Catalysts. The ICP-AES data in Table 1 demonstrate that the experimental copper contents are in good agreement with

DOI: 10.1021/cs5014909
ACS Catal. 2015, 5, 2088−2099

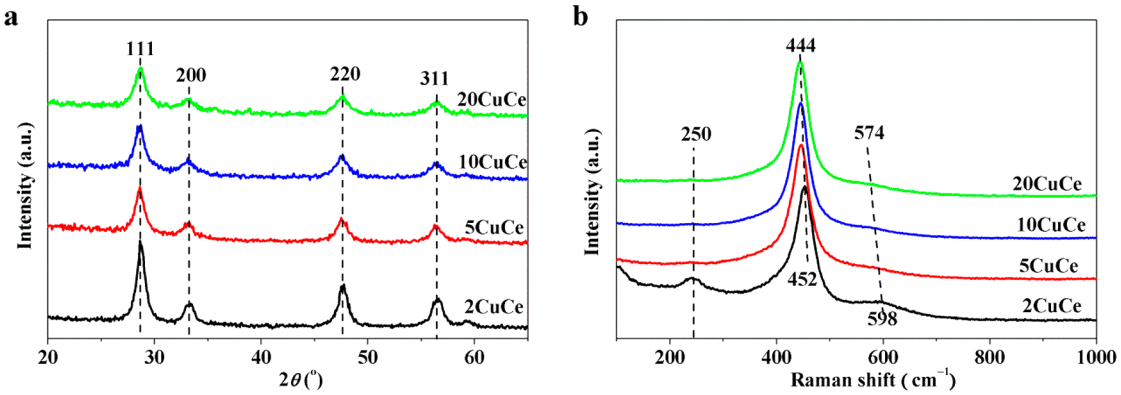

Figure 1. XRD patterns (a) and Raman spectra (b) of O_2-pretreated copper−ceria catalysts.

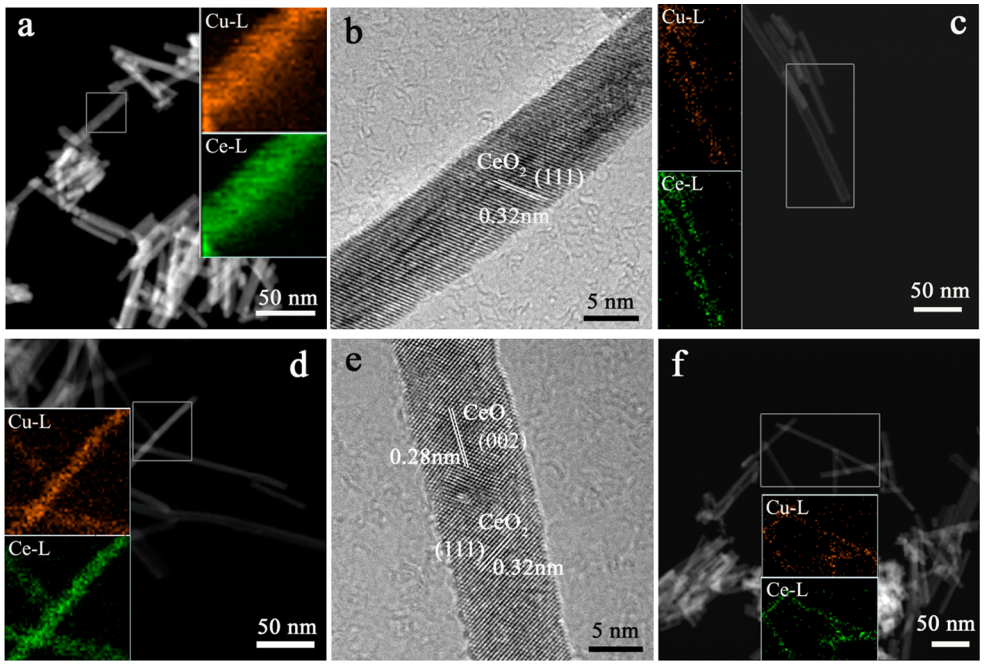

Figure 2. STEM (a, c, d, f) and HRTEM (b, e) images of O_2-pretreated copper−ceria catalyst: (a, b) 5CuCe, before PROX; (c) 5CuCe, after PROX; (d, e) 10CuCe, before PROX; (f) 10CuCe, after PROX. Insets are corresponding STEM-EDS elemental mapping images, and the ruling boxes on the STEM images indicate the data-collection areas.

those of designed values, confirming the successful Cu-loading implementation up to 20 wt %. The BET specific surface areas of fresh (air-calcined at 400 °C) copper−ceria catalysts vary from 80 to 97 $m^2 \cdot g^{-1}$ (see Table 1), which is consistent with the previous report on 15.4 at. % Cu loading on CeO_2 nanorods by the similar DP preparation (95 $m \cdot^2 g^{-1}$).[29]

The XRD patterns of the fresh copper−ceria samples in Figure 1a identify the presence of fcc Fluorite CeO_2 phase (JCPDS card no: 34-394) from 2CuCe to 20CuCe. The broadening of the diffraction patterns indicates the nanocrystalline nature of the ceria support. No diffraction peaks can be assigned to $Cu/Cu_2O/CuO$ structure, which reveals that no crystallized copper species isolated from the CeO_2 surface as high as the Cu amount up to 20 wt %.

To finely determine the crystal structure of fresh copper−ceria samples, Vis-Raman excited by a 532 nm laser was applied. Figure 1b distinctly exhibits the sharp peak centered at 444−452 cm^{-1}, corresponding to the triply degenerate F_{2g} mode of Fluorite CeO_2.[32] It has been reported that the Raman peak near 464 cm^{-1} in ceria nanoparticles shifts to lower energies and becomes broader and asymmetric as the particle size turns smaller,[33] and for doped ceria (Au/CeO_{2-x}), this peak decreases under the reducing atmosphere even down to <450 cm^{-1} when Ce^{3+} replaces Ce^{4+} during oxygen vacancy creation.[34] Our data in Figure 1b demonstrate that the deposition of copper helped the generation of oxygen vacancy in ceria, resulting in the low-energy shifts in Raman spectra. The other two wide bands at 250 and 574−598 cm^{-1} can be attributed to the presence of oxygen vacancies.[34,35] The related spectra in Figure 1b show that the Raman intensity of these two bands in 2CuCe is unreasonably higher than the other copper−ceria catalysts (5CuCe, 10CuCe, and 20CuCe). Because the confocal Raman measurement we applied is a microdomain technique (collection area: < 1 μm^2), it may not be good for the overall structural characterization on the low concentration (less than one monolayer) copper on the ceria nanorods, even we have investigated several (>5) spectra from different sample areas. Thus, other technique such as H_2-TPR (see this part below) is required to further confirm the above structural information on the copper−ceria catalysts. However, the

DOI: 10.1021/cs5014909
ACS Catal. 2015, 5, 2088−2099

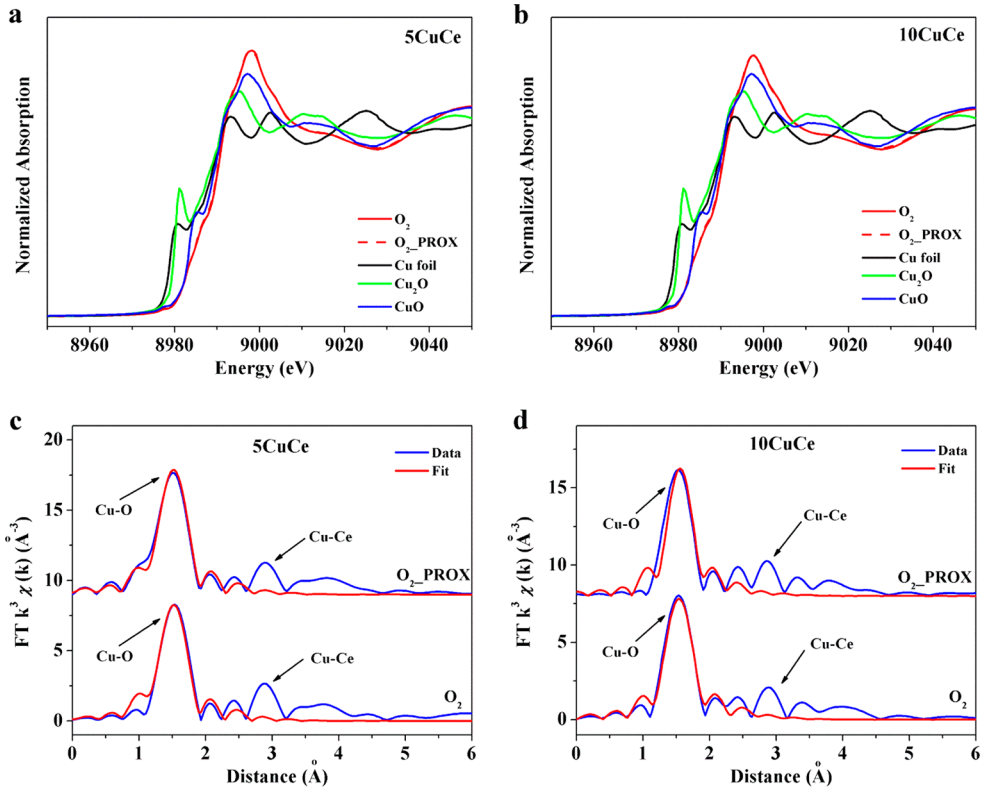

Figure 3. *In situ* XANES (a, b) and EXAFS *R* space (c, d) spectra of O_2-pretreated copper−ceria catalysts before and after CO-PROX reaction: (a, c) 5CuCe; (b, d) 10CuCe.

Table 2. XANES Analysis and EXAFS Fitting Results (*R*: Distance; CN: Coordination Number) of Copper−Ceria Catalysts

	molar fraction (%)[a]			Cu−O		Cu−Cu	
sample	Cu^0	Cu^+	Cu^{2+}	*R* (Å)	CN	*R* (Å)	CN
Cu[b]	—	—	—	—	—	2.56	12
Cu_2O[b]	—	—	—	1.85	4	3.70	8
CuO[b]	—	—	—	1.91 1.99	2 2	2.91	4
5CuCe (O_2)	—	0	100	1.93 ± 0.01	3.0 ± 0.3	—	—
5CuCe (H_2)	68 ± 3	32 ± 3	—	—	—	2.52 ± 0.01	3.8 ± 0.4
5CuCe (O_2, PROX)	—	0	100	1.94 ± 0.01	3.4 ± 0.2	—	—
5CuCe (H_2, PROX)	—	9 ± 3	91 ± 3	1.94 ± 0.01	2.2 ± 0.2	—	—
10CuCe (O_2)	—	0	100	1.94 ± 0.01	2.2 ± 0.3	—	—
10CuCe (H_2)	82 ± 3	18 ± 3	—	—	—	2.52 ± 0.01	5.0 ± 0.5
10CuCe (O_2, PROX)	—	0	100	1.94 ± 0.01	2.2 ± 0.2	—	—
10CuCe (H_2, PROX)	—	38 ± 2	62 ± 2	1.92 ± 0.03	1.5 ± 0.3	—	—

[a]Determined by XANES linear combination analysis with the Cu, Cu_2O, and CuO references. [b]EXAFS data (*R* and CN) were calculated by FEFF code from the crystal structures previous reported (JCPDS card#: 4-836, 5-667 and 41-254 for Cu, Cu_2O, and CuO, respectively).

separated CuO phase with Raman peaks located at 292, 340, and 626 cm^{-1} wavelengths[36] can be excluded.

To observe the morphology and crystal size/shape of copper−ceria catalysts from the microdomain view, the TEM characterization was carried out. STEM and HRTEM images on typical as-calcined samples have been shown in Figure 2. Typically, the fresh 5CuCe and 10CuCe were composed by nanorods with a length of 50−150 nm and a uniform width of ca. 10 nm (see Figure 2a,d). Figure 2b,e depicts the HRTEM images of a single nanorod, displaying the interplanar *d*-spacings for CeO_2 {111} (~0.32 nm) and {100} (~0.28 nm) facets. Similar to the related XRD results, no separated copper related (Cu/Cu_2O/CuO) nanostructures can be detected in HRTEM. Furthermore, elemental mapping analysis (insets in Figure 2a,d) from the corresponding STEM-EDS data confirm the homogeneous distribution of both Cu and Ce atoms in 5CuCe and 10CuCe. Therefore, based on the above experimental XRD, Vis-Raman, and TEM results, the fresh copper−ceria catalysts synthesized by the DP method in this work actually consisted of highly dispersed copper species supported on the CeO_2 nanorods.

The XAFS technique, which is also good for the structural detection of noncrystalline phase, was carried out to investigate the fresh copper−ceria catalysts. By the aid of copper standards (Cu foil, Cu_2O and CuO for Cu^0, Cu^+ and Cu^{2+}, respectively), the XANES profiles in Figure 3a,b clearly demonstrate the ionic

DOI: 10.1021/cs5014909
ACS Catal. 2015, 5, 2088−2099

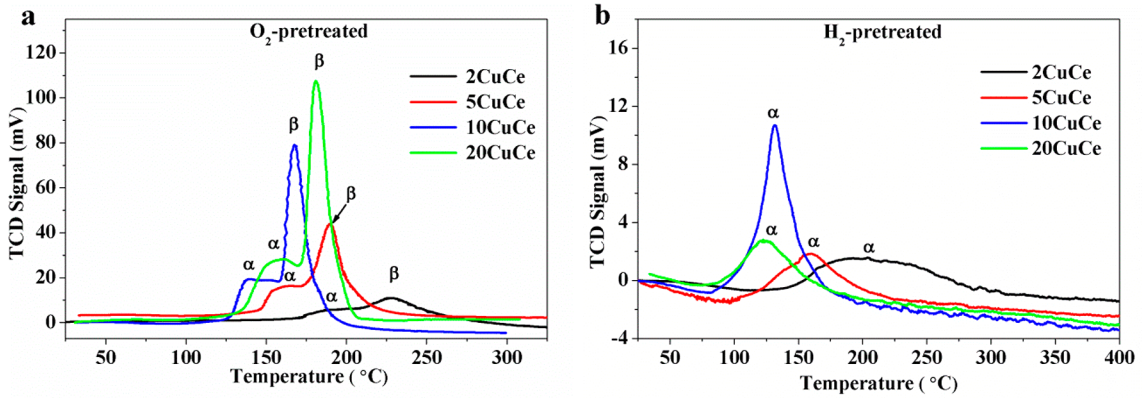

Figure 4. H_2-TPR profiles over copper−ceria catalysts: (a) O_2-pretreated; (b) H_2-pretreated.

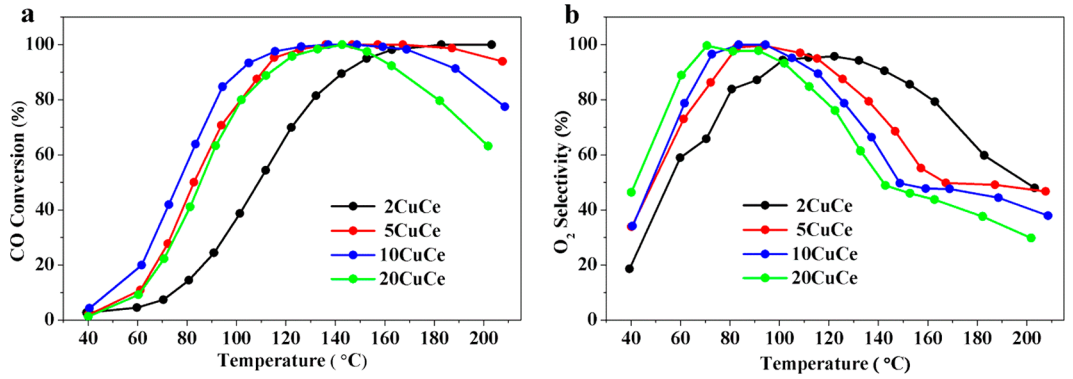

Figure 5. CO conversions (a) and O_2 selectivities (b) over O_2-pretreated copper−ceria catalysts.

Cu^{2+} feature for sample 5CuCe and 10CuCe. Meanwhile, by the aid of linear combination analysis,[37] negative molar fractions of either Cu^0 or Cu^+ species were eventually determined (see Table 2). The related EXAFS spectra in *R* space (see Figure 3c,d) display a strong contribution by the first shell of Cu−O at ca. 1.9 Å (phase shift corrected), which is different from the crystallized Cu_2O (one peak at 1.849 Å) or CuO (two peaks at 1.906 and 1.985 Å) phase (see Table 2 for modeling parameters). The corresponding coordination numbers (CN) obtained by the EXAFS fittings via the Artemis software are 3.0 and 2.2 for 5CuCe and 10CuCe, respectively (see Table 2). Although it cannot be fitted, the weak second shell around 3.3−3.4 Å in Figure 3c,d can be due to the Cu−Ce distance, which is very similar to the previous EXAFS results on the reported gold−ceria catalyst.[31]

In order to investigate the reducibility and identify the different surface oxygen species, H_2-TPR was carried out on the studied copper−ceria catalysts.[21,22,29,38] Figure 4a distinctly exhibits a two-step surface reduction process (also refer to Table 1 for values of reduction temperature and H_2 consumption) for each sample from 2CuCe to 20CuCe. The low-temperature wide band centered at 130−190 °C (α) was originated from the highly dispersed CuO_x clusters,[29,39] which is in good agreement with the first shell of Cu−O structure identified by the in situ EXAFS analysis (Figure 3c,d). However, the high-temperature sharp peak located at 190−230 °C (β) is due to the strong interaction of Cu−[O_x]−Ce structure,[29,40] which is consistent with the corresponding EXAFS fitting results, i.e., the appearance of Cu−Ce second shell in *R* space (see Figure 3c,d). Also, it can be seen in Figure 4a that sample 2CuCe exhibits reduction peaks obviously in a higher temperature range than the other three catalysts, possibly due to its stronger interaction between the CuO_x clusters and the ceria support.

The amount of H_2 globally consumed in each experiment increases with the copper loading. Meanwhile, the amount of hydrogen consumption is higher than the theoretical value according to the complete reduction of $Cu^{2+} \rightarrow Cu^0$ (see Table 1). It reveals that the surface oxygen bound to the ceria nanorods can also be reduced at low temperatures (<300 °C) by the aids of highly dispersed CuO_x (x = 0.2 − 0.5) clusters, which has been observed by other researchers previously.[41,42] Meanwhile, it can be seen from Table 1 that the higher copper loading, the less removable oxygen atoms (Cu/O ratio) in the catalysts. This can be explained that there is more fraction of strongly bound Cu−[O]$_x$−Ce (x = 0.7 − 3.2) species (β) which can activate more oxygen atoms on the surface of ceria, compared to the weakly bound CuO_x clusters (α), in the low Cu loading samples.

3.2. CO-PROX Reactivity of Copper−Ceria Catalysts.

To evaluate the catalytic performance of copper−ceria samples, the CO-PROX reaction was selected with a space velocity of 60 000 mL·g_{cat}^{-1}·h^{-1}. In experiments, CO oxidation (CO + O_2 → CO_2) is the target reaction; whereas H_2 oxidation (H_2 + O_2 → H_2O) is the side reaction to be minimized. Because the H_2 oxidation reactivity increases with the reaction temperature,[43] both CO conversion and O_2 selectivity under the working temperatures are very important to evaluate a PROX catalyst. Figure 5a,b display the CO conversions and O_2 selectivities of the studied catalysts after the preoxidation treatment (synthetic air, 300 °C, 30 min). It can be clearly seen that the CO conversion continuously increased with the copper content up

DOI: 10.1021/cs5014909
ACS Catal. 2015, 5, 2088−2099

Table 3. Comparison on CO-PROX Reactivity over Different Copper−Ceria Catalysts

sample	preparation	CO conv.	O_2 select.	reaction condition	ref
5 wt % Cu	DP	100% (120−170 °C)	100% (80−110 °C)	1%CO/1%O_2/50H_2/N_2, 60 000 mL·g_{cat}^{-1}·h^{-1}	this work
5 wt % Cu	CP	95% (150 °C)	100% (70−100 °C)	1%CO/1%O_2/H_2, 96 000 mL·g_{cat}^{-1}·h^{-1}	12
5 wt % Cu	DP	80% (170 °C)	100% (70−90 °C)	1%CO/1%O_2/H_2, 96 000 mL·g_{cat}^{-1}·h^{-1}	12
74 wt % Cu	CP	100% (120−200 °C)	100% (35−120 °C)	1%CO/1%O_2/50% H_2/N_2, 40 000 mL·g_{cat}^{-1}·h^{-1}	44
1 wt % Cu	IMP	100% (100−175 °C)	>97% (75−110 °C)	1%CO/1.25%O_2/50%H_2/He, 40 000 mL·g_{cat}^{-1}·h^{-1}	45
7 wt % Cu	sol−gel	100% (197 °C)	100% (150−200 °C)	1%CO/0.5%O_2/60%H_2/He, 12 000 mL·g_{cat}^{-1}·h^{-1}	20

to 10 wt %, followed by a small decrease for 20CuCe (see Figure 5a). Nearly full conversion was achieved for 5CuCe to 10CuCe at 120 °C. On the other hand, the appropriate temperature window for selectivity was 80−110 °C on 5CuCe or 10CuCe, displaying high O_2-selectivities more than 90% (see Figure 5b). Under the O_2-pretreatment condition, the best copper−ceria catalysts with perfect catalytic performance were sample 5CuCe and 10CuCe, i.e., 90−95% O_2 selectivity with nearly full CO conversion at 115 °C.

Actually, our copper−ceria catalysts are rather active for the CO-PROX reaction, if compared to those in the literature (see Table 3). As a good PROX catalyst, the optimized reaction temperatures should be as close as possible between CO conversion and O_2 selectivity. A nearly full CO conversion in a wide temperature window (120−170 °C) compared to the previous 5 wt %Cu−CP,[12] DP[12] and 7 wt %Cu−sol−gel samples,[20] and higher O_2 selectivity nearly 100% at temperatures of 80−110 °C than almost all samples except 74 wt % Cu−CP[44] and 1 wt %Cu on ceria nanocubes prepared by the impregnation method,[45] which can efficiently abate CO concentration to acceptable levels for the PEMFC operating at 80−140 °C, Thus, excellent catalytic performance for the CO-PROX reaction has been confirmed over the highly dispersed CuO_x clusters supported on the CeO_2 nanorods.

3.3. Active Species of Copper−Ceria Catalysts for CO-PROX Reaction. Considering the harsh testing conditions, especially the strong reducing atmosphere (1%CO/1%O_2/50% H_2/N_2), were there structural and/or textural changes of the copper−ceria catalysts after the CO-PROX reaction? The XRD patterns of the used copper−ceria catalysts in Figure S1a reveal that no separated Cu phase was generated for the low-concentration copper loadings up to 10 wt %. The TEM measurements were applied for the used 5CuCe and 10CuCe samples to check if there was any textural evolution during the catalytic tests. From the STEM images in Figure 2c,f, the morphology and crystal shape/size were maintained for copper supported onto ceria nanorods. Furthermore, the corresponding elemental mapping pictures confirm that the Cu and Ce species were homogeneously distributed and that there was no obvious Cu-rich or Ce-rich region. Figure S2a,b depict the HRTEM images of the 5CuCe and 10CuCe samples; only lattice formation on CeO_2 was observed, and no separated copper ($Cu/Cu_2O/CuO$) nanostructures can be identified in HRTEM. Thus, copper was still highly dispersed on the rod-like CeO_2 support for 5CuCe and 10CuCe after the CO-PROX test.

The *in situ* technique is very important to reveal the active site of the catalyst and the mechanism or pathway of catalytic reaction. Very recently, Yao et al. reported the importance of novel operando combined XANES (fluorescence) and DRIFTS characterization for the dynamic structural detection on 5 wt % CuO/CeO_2 nanorods prepared by the impregnation method for the transient CO oxidation process without the presence of H_2 gas (3.3%CO/1.7%O_2/95%He).[27] They identified the surface dispersed Cu(I) rather than Cu(0) as active species; however, the local coordination structures of the active species were unknown due to the low signal-to-noise level under short collection time (380 s per scan). Although CO-PROX is also essentially the CO oxidation reaction, the presence of H_2 with very high concentration (50%) in the reaction gas can greatly influence the catalytic behavior/mechanism of the catalyst. Meanwhile, CO-PROX also induces a second reaction of H_2 oxidation, which makes it necessary to consider this situation effect to the active species in the CuO/CeO_2 catalyst. As we have mentioned, XANES is effective for the determination of electronic structure (oxidation state, charge transfer, etc.), whereas EXAFS provides short-range local structural information such as coordination number, bond distance, and so on, which is more crucial to explore the interaction between copper species and the ceria support in catalysis. Therefore, in our work, both *in situ* XANES and *in situ* EXAFS measurement under the "steady state" CO-PROX reaction conditions were carried out to study the structural evolution on the measured copper−ceria samples prepared by the deposition−precipitation method. The reaction temperature for each test was fixed at 80 °C, which exhibits moderate CO conversions over the measured copper−ceria catalysts from the related "light off" profiles in Figure 5a. The XANES profiles in Figure 3a,b (dash lines, overlapped with solid lines) show that the oxidation state of copper was maintained as copper(II) for 5CuCe and 10CuCe after the reaction, and the corresponding linear combination analyses confirm the pure Cu^{2+} component (see Table 2). These observations are different from those documented in Yao et al's work,[27] where both Cu(II) and Cu(I) were observed during the CO oxidation reaction study with a stoichiometric feed comprising of 3.3%CO/1.7%O_2/He. This difference on the nature of active copper sites could arise from the different composition of the reaction feed gases used in this work and in previous report.[27] Therefore, Cu(II) could be reduced to Cu(I) by the CO gas during the reaction (100 °C).[27] One might wonder that the presence of a large excess of hydrogen in the feed gas of the present work (1%CO/1%O_2/ 50%H2/N_2) would also lead to Cu(II) reduction, even though the CO concentration is lower than that in Yao et al's work.[27] This wondering would be reasonably excluded on consideration of the TPR results shown in Figure 4, which clearly show that H_2 was unable to reduce Cu(II) at the temperature of our measurement (80 °C). The EXAFS fitting results in Figure 3c,d determine the contribution by Cu−O (1st shell, major) and Cu−Ce (2nd shell, minor), the same as the fresh catalysts after O_2-pretreatment. Significantly, the fitted values for CN of Cu−O shell in Table 2 show no differences between the fresh (5CuCe: 3.0; 10CuCe: 2.2) and the used samples (5CuCe: 3.4; 10CuCe: 2.2). It gives a hint that both the highly dispersed CuO_x cluster and the strong interaction of Cu−[O_x]−Ce

DOI: 10.1021/cs5014909
ACS Catal. 2015, 5, 2088−2099

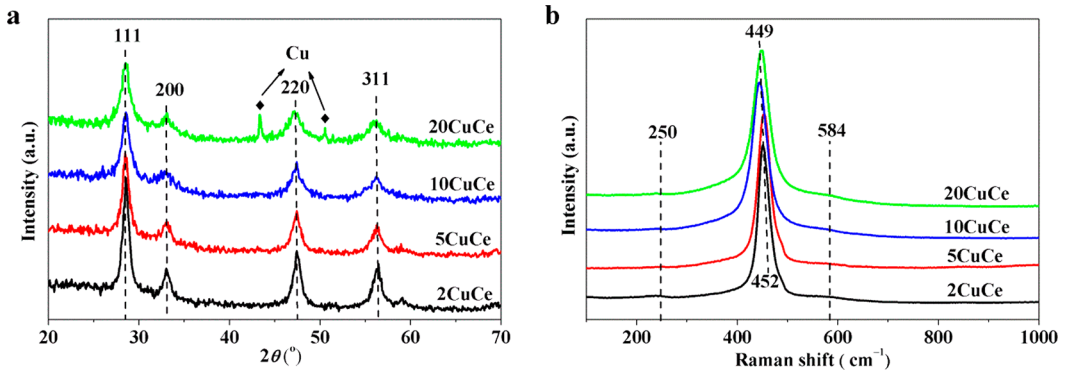

Figure 6. XRD patterns (a) and Raman spectra (b) of H_2-pretreated copper−ceria catalysts.

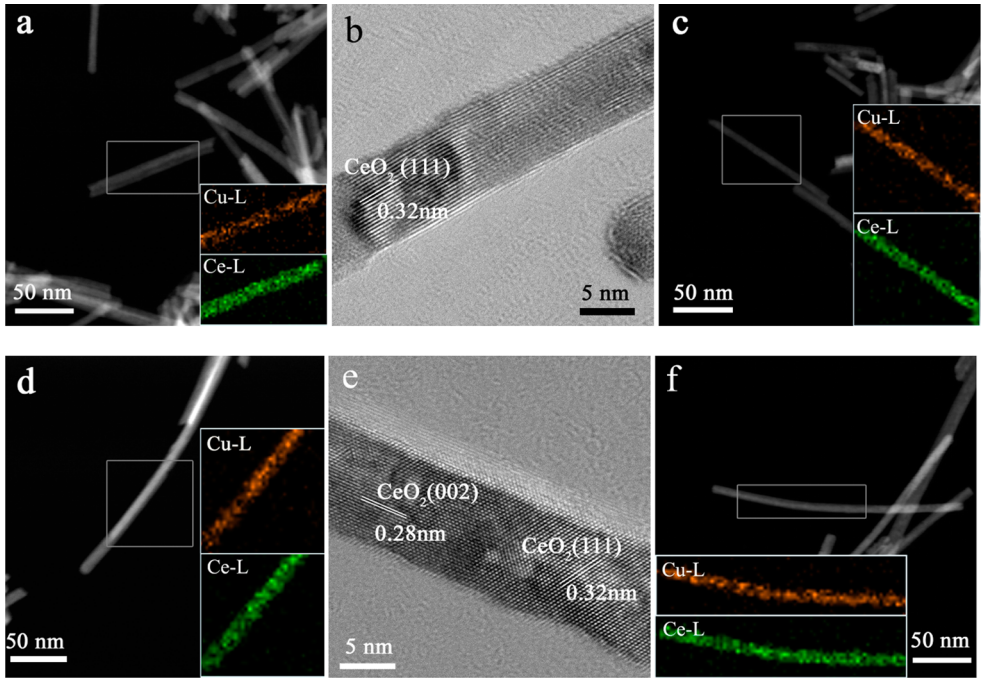

Figure 7. STEM (a, c, d, f) and HRTEM (b, e) images of H_2-pretreated copper−ceria catalyst: (a, b) 5CuCe, before PROX; (c) 5CuCe, after PROX; (d, e) 10CuCe, before PROX; (f) 10CuCe, after PROX. Insets are corresponding STEM-EDS elemental mapping images, and the ruling boxes on the STEM images indicate the data-collection areas.

structure were totally maintained during the CO-PROX reaction.

To further distinguish the effect of the above two copper species, we carried out a prereduction treatment on typical catalysts, with the aim to eliminate the positively charged copper species before the CO-PROX reaction. The XRD patterns of H_2-pretreated copper−ceria catalysts in Figure 6a indicate that CeO_2 fluorite structure was kept for the low-concentration copper loadings (up to 10 wt %) after the prereduction, whereas an isolated metallic Cu phase formed for 20CuCe. The related Raman spectra in Figure 6b confirm the absence of separated copper oxide structure from 2CuCe to 10CuCe. From the HRTEM images in Figure 7, the CeO_2 rod-like shape as well as the related crystal size was maintained for H_2-pretreated 5CuCe (Figure 7b) and 10CuCe (Figure 7e).

Furthermore, the corresponding STEM-EDS elemental mapping results in Figure 7a,d clearly depict that the Cu and Ce species were highly dispersed on the support surface, and no obvious Cu-rich or Ce-rich region was observed for the prereduced 5CuCe and 10CuCe catalysts. Therefore, based on the above characterization results, we can verify that the copper species, up to 10 wt % Cu, were still highly dispersed on the ceria support after the H_2-pretreatment. We noticed the strange behavior of 20CuCe, which not only formed isolated metallic Cu phase after the H_2-pretreatment but also deviated from the trend of investigated copper−ceria catalysts (i.e., lower reduction temperature in H_2-TPR and higher CO conversion in PROX with the increase of Cu content). This could be caused by the partial coverage of active sites for reaction/reduction at the high copper loading.

The *in situ* XAFS results in Figure 8 clearly exhibit the formation of dominant metallic Cu clusters/particles with a CN of Cu−Cu (distance: ca. 2.5 Å) in the range of 3.8−5.0, plus the minor Cu−O shell remained (refer to Table 2). This confirms the effective but uncompleted reduction of oxidized copper species in the fresh samples after 300 °C in 20%H_2/He. Meanwhile, the Cu−Ce shell in the preoxidized catalysts was removed by the hydrogen molecules during the reduction (see Figure 8c,d). To further verify the total elimination of strongly bound Cu−[O_x]−Ce species, the related H_2-TPR tests were

DOI: 10.1021/cs5014909
ACS Catal. 2015, 5, 2088−2099

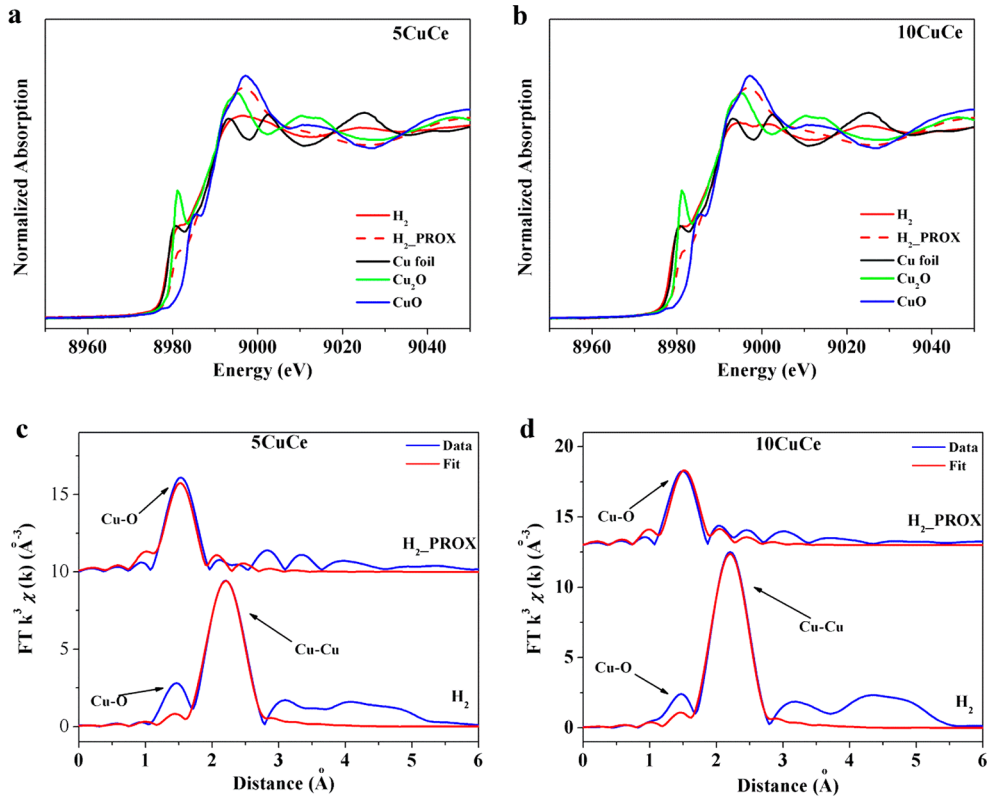

Figure 8. *In situ* XANES (a, b) and EXAFS *R* space (c, d) spectra of H_2-pretreated copper−ceria catalysts before and during PROX reaction: (a, c) 5CuCe; (b, d) 10CuCe.

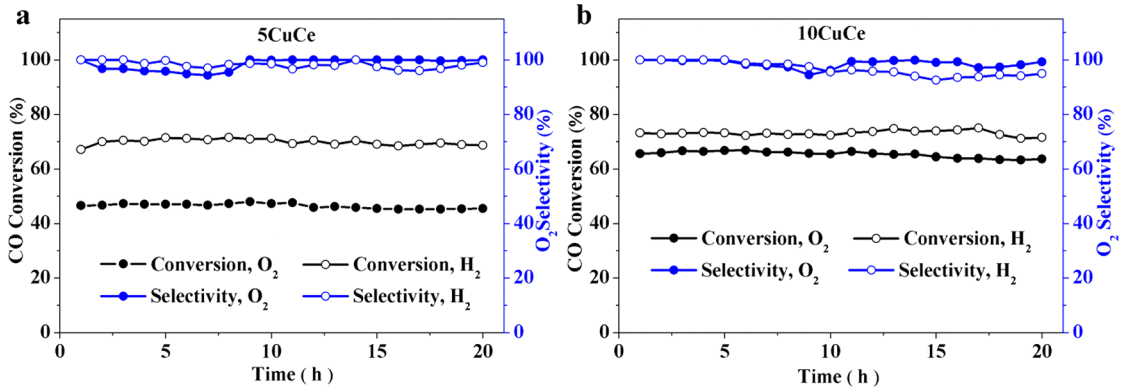

Figure 9. Stability tests of copper−ceria catalysts: (a) 5CuCe; (b) 10CuCe. Reaction conditions: 1%CO/1%O_2/50%H_2/N_2, at 80 °C, SV = 60 000 mL·h^{-1}·g_{cat}^{-1}.

carried out on the H_2-pretreated catalysts, without any further pretreatment between prereduction and TPR measurement. Figure 4b, together with the corresponding comparison results in Figure S3, clearly exhibits that the reduction peak areas of the H_2-pretreated copper−ceria samples were significantly lower than those of the O_2-pretreated samples. Most importantly, the high-temperature reduction with sharp line shape (Cu−[O_x]−Ce, β in Figure 4) completely disappeared after the H_2-pretreatment, and the low-temperature reduction with a broad profile (CuO_x, α in Figure 4) remained. These results are in good agreement with the corresponding XAFS analysis in Figure 8.

After the "steady-state" in situ CO-PROX reaction at 80 °C for 1 h, the H_2-pretreated 5CuCe and 10CuCe samples maintained the same structure as the prereduced catalysts before reaction, if considering the related XRD (Figure S1b) and TEM results (Figure 7c,f and S2c,d). Interestingly, the prereduced copper−ceria catalyst was partially reoxidized under the PROX reaction conditions (1%CO/1%O_2/50%H_2/He, 80 °C, 1 h). The corresponding XANES profiles in Figure 8a,b display the redispersion of $Cu^{\delta+}$ (δ = 1−2) species (also refer to the linear combination analysis in Table 2), and the related EXAFS spectra in Figure 8c,d confirm the formation of strong Cu−O shell after the H_2 → CO-PROX cycle for 5CuCe and 10CuCe. It demonstrates that the CO oxidation reaction was dominant, which kept the ionic copper structure; however, the H_2 oxidation was minimized at the reaction temperature of 80 °C and the $Cu^{\delta+}$ species were unable to be reduced even by high-concentration (50%) H_2. Similar phenomena have been observed and attributed to the presence of Cu^+-carbonyl

DOI: 10.1021/cs5014909
ACS Catal. 2015, 5, 2088−2099

intermediate confirmed by in situ DRIFTS.[26] The linear combination analysis in Table 2 indicates that the minor fraction of Cu^+ (9% for 5CuCe and 38% for 10CuCe) was determined after such H_2-PROX process. Since XAFS averaged the contribution by both Cu^{2+} and Cu^+ species in our system, this characterization may miss the experimental evidence on verifying the role of Cu(I) for PROX, which has been previously revealed by the in situ DRIFTS characterization.[18,26]

However, the second Cu−Ce shell caused by the strong interaction of the Cu−[O_x]−Ce structure was unable to be recovered (Figure 8c,d). In other words, only highly dispersed CuO_x clusters were reversible species during the H_2 → CO-PROX process. Thus, the newly formed oxidized copper species after H_2-PROX were actually different from those created in the preoxidized catalysts. Meanwhile, the fitted values on CN of Cu−O shell after the prereduction and the sequential CO-PROX reaction were 2.2 and 1.5 for 5CuCe and 10CuCe, respectively. These coordination numbers were significantly lower than those of the preoxidized or O_2-PROX (see Table 2), revealing that the Cu−[O_x]−Ce structure was also attributed to the formation of first Cu−O shell in fresh or O_2-PROX samples. Previously, for the copper−ceria catalyst on the CO-PROX reaction, Daniel Gamarra et al. applied an in situ XANES analysis, as well as the operando DRIFTS measurement to identify the active sites as the interfacial positions of the dispersed copper oxide entities.[26] In our work, the related EXAFS fittings in *R* space played a crucial role in distinguishing two similar copper oxide species (i.e., highly dispersed CuO_x clusters and strong interaction of Cu−[O_x]−Ce structure), on the basis of which the active sites of copper−ceria catalysts for the CO-PROX reaction were identified.

Figure 9 exhibits the long-term stability tests on either preoxidized or prereduced copper−ceria catalysts. All of the O_2-selectivities were close to 100% for 5CuCe and 10CuCe, regardless of O_2- or H_2-pretreatment (also refer to Table 1). For CO conversion, the prereduced samples were significantly enhanced if compared to the preoxidized catalysts (see Figure 9 and Table 1) for 5CuCe (48% → 70%), and slightly improved for 10CuCe (65% → 72%) after 20 h of measurement. Thus, the H_2-pretreatment indeed benefited the catalytic reactivity of the present copper−ceria samples for CO-PROX more than the O_2-pretreatment, especially for the catalysts with relatively low Cu content. Based on the above in situ XAFS results, this promotion effect is related to the following aspects: the elimination of Cu−[O_x]−Ce species, and the recovery or even enhancement of CuO_x clusters. All the above verify that the activity of CO conversion of copper−ceria catalyst for the CO-PROX reaction can be attributed to the highly dispersed CuO_x clusters, instead of the strongly bound Cu−[O_x]−Ce species.

For the studies on "structure−activity" relationship in Cu−Ce−O system for the CO-PROX reaction, previously, extensive investigation has been carried out in the past two decades, and many different modes have been proposed regarding the nature of the active sites. Among them, the active species of the catalysts have been argued in debates. Liu and Flytzani-Stephanopoulos found that the strong interaction and synergism of Cu−CeO_2 catalysts were sufficient to promote the catalytic activity of CO.[46] In 2000, Martinez-Arias et al. reported the presence of highly dispersed CuO entities and determined the dispersion degree by the XRD, XPS, and XAFS characterizations.[47] Then, Gamarra et al. demonstrated that CO oxidation took place at interfacial positions of the dispersed copper oxide entities, and active species must be mainly related to partially reduced (e.g., Cu^+) dispersed copper oxide nanoparticles.[26] In 2007, Luo et al. identified the finely dispersed CuO phase, the bulk CuO particles, and the Cu^{2+} ions in the CeO_2 lattice and further studied the corresponding evolution between these three different copper species.[48] Therefore, for Cu−O−Ce catalyst in CO-PROX, still no perfect and recognized model has been obtained.

Based on the above discussion on the corresponding structural characterization (XRD, Vis-Raman, TEM, H_2-TPR and XAFS) and catalytic tests for the O_2- or H_2-pretreated copper−ceria catalysts, we now have a full image of "structure−activity" relationship in the Cu−Ce−O system for CO-PROX (see Scheme 1): (1) The preoxidized sample consisted of highly dispersed CuO_x clusters, plus strong interaction of Cu−[O_x]−Ce, which has been demonstrated by the in situ EXAFS fittings (1st Cu−O and second Cu−Ce shells), as well as the H_2-TPR data; (2) The related copper species in the preoxidized catalyst were maintained after the CO-PROX reaction, and no significant differences on XAFS characterization have been observed; (3) The prereduction step effectively removed the positively charged copper components (Cu^+ and Cu^{2+}), and Cu nanoparticles with a low coordination number (<5) of Cu−Cu shell were created; (4) Highly dispersed CuO_x clusters, instead of the strongly bound Cu−[O_x]−Ce species, were recovered after the H_2 → CO-PROX process, and the corresponding CO conversion and O_2 selectivity were clearly enhanced if compared to those of the preoxidized sample. Therefore, it can be concluded that the highly dispersed CuO_x clusters in copper−ceria catalysts are the crucial active species for the CO-PROX reaction. Here, ceria is a good reducible support for copper deposition and acts as a stabilizer for highly dispersed copper oxide species. Both CuO_x and Cu−[O_x]−Ce species have active oxygen ions attached to Cu center, which can be probed by low-temperature surface reduction in H_2-TPR because the removal of surface oxygen in pure ceria happens above 300 °C.[49]

Scheme 1. Schematic Demonstration on Structural Evolutions of Highly Dispersed Copper on Ceria Nanorods for the CO-PROX Reaction

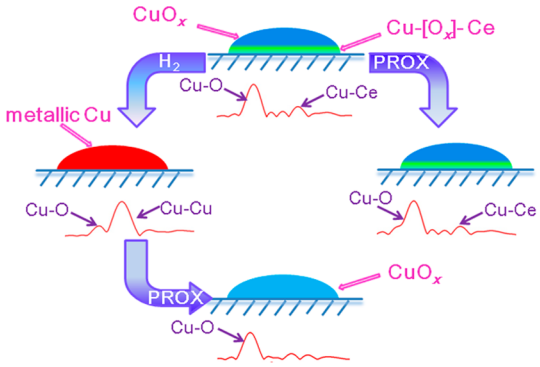

4. CONCLUSION

This work showed that our preparation by deposition-precipitation of copper catalyst on supporting ceria nanorods has led to uniformly dispersed copper oxide on the ceria surface up to 10 wt% Cu loading. Insight into the evolution of active copper sites for CO-PROX reaction has been provided based on the in-situ XANES/EXAFS measurements. The reaction over the O_2-pretreated catalysts was shown to proceed with

DOI: 10.1021/cs5014909
ACS Catal. 2015, 5, 2088−2099

Cu(II) as the solely active state; however, a mixed Cu(II)/Cu(I) states, with Cu(II) being the dominant state, were observed to serve the reaction over the H_2-pretreated catalysts. Coexistence of highly dispersed CuO_x clusters and Cu-[O_x]-Ce entities strongly bound with the support were discerned in the samples. The pre-reduction with H_2 resulted in breaking of the Cu-[O_x]-Ce binding and significantly enhanced catalytic activity, demonstrating that the highly dispersed surface CuO_x clusters rather than Cu-[O_x]-Ce are more crucial to the CO-PROX reaction.

■ ASSOCIATED CONTENT

Supporting Information

The following file is available free of charge on the ACS Publications website at DOI: 10.1021/cs5014909.

XRD patterns and HRTEM images on the used catalysts, and comparison on H_2-TPR profiles between O_2-pretreated and H_2-pretreated samples (PDF)

■ AUTHOR INFORMATION

Corresponding Authors

*E-mail: sirui@sinap.ac.cn.
*E-mail: jiacj@sdu.edu.cn.

Notes

The authors declare no competing financial interest.

■ ACKNOWLEDGMENTS

Financial supported from the National Science Foundation of China (NSFC) (grant nos. 21301107, 21373259, 21331001 and 11079005), Fundamental research funding of Shandong University (grant nos. 2014JC005), the Taishan Scholar project of Shandong Province (China), Open Funding from Beijing National Laboratory for Molecular Science, the Hundred Talents project of the Chinese Academy of Sciences, the Strategic Priority Research Program of the Chinese Academy of Sciences (grant no. XDA09030102). We thank Nebojsa Marinkovic (University of Delaware) for his kind help on the in situ XAFS setups.

■ REFERENCES

(1) Tada, M.; Bal, R.; Mu, X. D.; Coquet, R.; Namba, S.; Iwasawa, Y. *Chem. Commun.* **2007**, *44*, 4689−4691.
(2) Zhang, R.; Haddadin, T.; Rubiano, D. P.; Nair, H.; Polster, C. S.; Baertsch, C. D. *ACS Catal.* **2011**, *1*, 519−525.
(3) Choudhary, T. V.; Goodman, D. W. *Catal. Today* **2002**, *77*, 65−78.
(4) Kotobuki, M.; Watanabe, A.; Uchida, H.; Yamashita, H.; Watanabe, M. *J. Catal.* **2005**, *236*, 262−269.
(5) Korotkikh, O.; Farrauto, R. *Catal. Today* **2000**, *62*, 249−254.
(6) Kim, D. H.; Lim, M. S. *Appl. Catal., A* **2002**, *224*, 27−38.
(7) Avgouropoulos, G.; Ioannides, T.; Papadopoulou, C.; Batista, J.; Hocevar, S.; Matralis, H. *Catal. Today* **2002**, *75*, 157−167.
(8) Marino, F.; Descorme, C.; Duprez, D. *Appl. Catal., B* **2004**, *54*, 59−66.
(9) Snytnikov, P. V.; Sobyanin, V. A.; Belyaev, V. D.; Tsyrulnikov, P. G.; Shitova, N. B.; Shlyapin, S. A. *Appl. Catal., A* **2003**, *239*, 149−156.
(10) Kim, Y. H.; Park, E. D.; Lee, H. C.; Lee, D.; Lee, K. H. *Catal. Today* **2009**, *146*, 253−259.
(11) Landon, P.; Ferguson, J.; Solsona, B. E.; Garcia, T.; Carley, A. F.; Herzing, A. A.; Kiely, C. J.; Golunski, S. E.; Hutchings, G. J. *Chem. Commun.* **2005**, *27*, 3385−3387.
(12) Scirè, S.; Crisafulli, C.; Riccobene, P. M.; Patanè, G.; Pistone, A. *Appl. Catal., A* **2012**, *417*, 66−75.
(13) Han, Y. F.; Kahlich, M. J.; Kinne, M.; Behm, R. J. *Phys. Chem. Chem. Phys.* **2002**, *4*, 389−397.
(14) Caputo, T.; Lisi, L.; Pirone, R.; Russo, G. *Appl. Catal., A* **2008**, *348*, 42−53.
(15) Fonseca, J. D. L.; Ferreira, H. S.; Bion, N.; Pirault-Roy, L.; Rangel, M. D.; Duprez, D.; Epron, F. *Catal. Today* **2012**, *180*, 34−41.
(16) Gu, D.; Jia, C. J.; Bongard, H.; Spliethoff, B.; Weidenthaler, C.; Schmidt, W.; Schüth, F. *Appl. Catal., B* **2014**, *152*, 11−18.
(17) Moretti, E.; Lenarda, M.; Riello, P.; Storaroa, L.; Talon, A.; Frattini, R.; Reyes-Carmona, A.; Jimenez-Lopez, A.; Rodriguez-Castellon, E. *Appl. Catal., B* **2013**, *129*, 556−565.
(18) Gamarra, D.; Munuera, G.; Hungría, A. B.; Fernández-García, M.; Conesa, J. C.; Midgley, P. A.; Wang, X. Q.; Hanson, J. C.; Rodríguez, J. A.; Martínez-Arias, A. *J. Phys. Chem. C* **2007**, *111*, 11026−11038.
(19) Jia, A. P.; Hu, G. S.; Meng, L.; Xie, Y. L.; Lu, J. Q.; Luo, M. F. *J. Catal.* **2012**, *289*, 199−209.
(20) Gurbani, A.; Ayastuy, J. L.; González-Marcos, M. P.; Gutiérrez-Ortiz, M. A. *Int. J. Hydrogen Energy* **2010**, *35*, 11582−11590.
(21) Han, J.; Kim, H. J.; Yoon, S.; Lee, H. *J. Mol. Catal. A-Chem.* **2011**, *335*, 82−88.
(22) Polster, C. S.; Nair, H.; Baertsch, C. D. *J. Catal.* **2009**, *266*, 308−319.
(23) Ciston, J.; Si, R.; Rodriguez, J. A.; Hanson, J. C.; Martínez-Arias, A.; Fernandez-García, M.; Zhu, Y. M. *J. Phys. Chem, C* **2011**, *115*, 13851−13859.
(24) Hornès, A.; Hungría, A. B.; Bera, P.; López Cámara, A.; Fernández-García, M.; Martínez-Arias, A.; Barrio, L.; Estrella, M.; Zhou, G.; Fonseca, J. J.; Hanson, J. C.; Rodriguez, J. A. *J. Am. Chem. Soc.* **2010**, *132*, 34−35.
(25) Gamarra, D.; Fernández-García, M.; Belver, C.; Martínez-Arias, A. *J. Phys. Chem. C* **2010**, *114*, 18576−18582.
(26) Gamarra, D.; Belver, C.; Fernández-García, M.; Martínez-Arias, A. *J. Am. Chem. Soc.* **2007**, *129*, 12064−12065.
(27) Yao, S. Y.; Mudiyanselage, K.; Xu, W. Q.; Johnston-Peck, A. C.; Hanson, J. C.; Wu, T. P.; Stacchiola, D.; Rodriguez, J. A.; Zhao, H. Y.; Beyer, K. A.; Chapman, K. W.; Chupas, P. J.; Martínez-Arias, A.; Si, R.; Bolin, T. B.; Liu, W. J.; Senanayake, S. D. *ACS Catal.* **2014**, *4*, 1650−1661.
(28) Zhang, R.; Miller, J. T.; Baertsch, C. D. *J. Catal.* **2012**, *294*, 69−78.
(29) Si, R.; Raitano, J.; Yi, N.; Zhang, L. H.; Chan, S. W.; Flytzani-Stephanopoulos, M. *Catal. Today* **2012**, *180*, 68−80.
(30) Mai, H. X.; Sun, L. D.; Zhang, Y. W.; Si, R.; Feng, W.; Zhang, H. P.; Liu, H. C.; Yan, C. H. *J. Phys. Chem. C* **2005**, *109*, 24380−24385.
(31) Deng, W. L.; Frenkel, A. L.; Si, R.; Flytzani-Stephanopoulos, M. *J. Phys. Chem. C* **2008**, *112*, 12834−12840.
(32) Weber, W. H.; Hass, K. C.; McBride, J. R. *Phys. Rev. B* **1993**, *48*, 178−185.
(33) Spanier, J. E.; Robinson, R. D.; Zhang, F.; Chan, S. W.; Herman, I. P. *Phys. Rev. B* **2001**, *64*, 245407.
(34) Lee, Y.; He, G. H.; Akey, A. J.; Si, R.; Flytzani-Stephanopoulos, M.; Herman, I. P. *J. Am. Chem. Soc.* **2011**, *133*, 12952−12955.
(35) McBride, J. R.; Hass, K. C.; Poindexter, B. D.; Weber, W. H. *J. Appl. Phys.* **1994**, *76*, 2435−2441.
(36) Gamboa-Rosales, N. K.; Ayastuy, J. L.; Gonzalez-Marcos, M. P.; Gutiérrez-Ortiz, M. A. *Int. J. Hydrogen Energy* **2012**, *137*, 7005−7016.
(37) Frenkel, A. I.; Wang, Q.; Marinkovic, N.; Chen, J. G.; Barrio, L.; Si, R.; Cámara, A. L.; Estrella, A. M.; Rodriguez, J. A.; Hanson, J. C. *J. Phys. Chem. C* **2011**, *115*, 17884−17890.
(38) Yen, H.; Seo, Y.; Kaliaguine, S.; Kleitz, F. *Angew. Chem., Int. Ed.* **2012**, *51*, 12032−12035.
(39) Kundakovic, L.; Flytzani-Stephanopoulos, M. *Appl. Catal., A* **1998**, *171*, 13−29.
(40) Kundakovic, L.; Flytzani-Stephanopoulos. *J. Catal.* **1998**, *179*, 203−221.
(41) Tang, X. L.; Zhang, B. C.; Li, Y.; Xu, Y. D.; Xin, Q.; Shen, W. J. *Appl. Catal., A* **2005**, *288*, 116−125.

(42) Zimmer, P.; Tschope, A.; Birringer, R. *J. Catal.* **2002**, *205*, 339−345.
(43) Kahlich, M. J.; Gasteiger, H. A.; Behm, R. J. *J. Catal.* **1999**, *182*, 430−440.
(44) Zeng, S. H.; Zhang, W. L.; Sliwa, M.; Su, H. Q. *Int. J. Hydrogen Energy* **2013**, *38*, 3597−3605.
(45) Gamarra, D.; Camara, A. L.; Monte, M.; Rasmussen, S. B.; Chinchilla, L. E.; Hungria, A. B.; Munuera, G.; Gyorffy, N.; Schay, Z.; Corberan, V. C.; Conesa, J. C.; Martinez-Ariasa, A. *Appl. Catal., B* **2013**, *130*, 224−238.
(46) Liu, W.; Flytzani-Stephanopoulos, M. *Chem. Eng. J.* **1996**, *64*, 283−294.
(47) Martínez-Arias, A.; Fernández-García, M.; Gálvez, O.; Coronado, J. M.; Anderson, J. A.; Conesa, J. C.; Soria, J.; Munuera, G. *J. Catal.* **2000**, *195*, 207−216.
(48) Luo, M. F.; Song, Y. P.; Lu, J. Q.; Wang, X. Y.; Pu, Z. Y. *J. Phys. Chem. C* **2007**, *111*, 12686−12692.
(49) Fu, Q.; Weber, A.; Flytzani-Stephanopoulos, M. *Catal. Lett.* **2001**, *77*, 87−95.

DOI: 10.1021/cs5014909
ACS Catal. 2015, 5, 2088−2099